Cancer Chemother Pharmacol (2008) 62:337–346
DOI 10.1007/s00280-007-0637-y

ORIGINAL ARTICLE

Mechanisms of enhanced tumoricidal efficacy of multiple small dosages of ranpirnase, the novel cytotoxic ribonuclease, on lung cancer

Intae Lee · Kuslima Shogen

Received: 7 July 2007 / Accepted: 24 October 2007 / Published online: 5 December 2007

Abstract
Purpose The effect of multiple small dosages of the cytotoxic RNase, ranpirnase (ONCONASE®, ONC), on lung cancer was studied. The possible mechanisms for the enhanced tumoricidal efficacy of multiple small dosages of ONC were also investigated.
Methods Hematoxylin and eosin staining, TUNEL labeling, and caspase-3-antibody labeling were used for in vivo analysis of apoptosis. A growth-delay assay was applied to detect the therapeutic potential of small and multiple dosages of ONC in vivo. ONC-induced changes in blood flow in A549 tumors and the kidney were measured non-invasively by dynamic contrast enhanced magnetic resonance imaging (DCE-MRI).
Results In cell culture studies, ONC significantly inhibited tumor growth of A549 human NSCLC cells without damaging non-cancerous cells (HLF-1 human lung fibroblast). Multiple small dosages of ONC significantly prolonged tumor growth delay of A549 tumors, with increased apoptosis in vivo from 0.5 ± 0.3 to 70.1 ± 1.1% (by TUNEL labeling, $N = 3$, $P < 0.05$). Interestingly, multiple small doses of ONC were more effective than a single large dose for the inhibition of tumor growth with reduced side effect. Using non-invasive DCE-MRI methods, we found that the mean of the K^{trans} median values increased to 49.3 ± 7.5% from the pre-ONC values by ONC ($N = 4$ mice, $P < 0.05$). A subsequent T_1 map of the kidney showed that T_1 values were temporarily decreased for up to 2 days (however, fully recovered ~4 days post-treatment).
Conclusions Multiple small dosages of ONC significantly inhibited tumor growth of A549 NSCLC cells in vivo, with markedly increased apoptosis. This investigation suggests important potential clinical uses of ONC for the treatment of NSCLC cancer patients.

Keywords Lung cancer · Cytotoxic RNase · Ranpirnase · Onconase®

I. Lee (✉)
Department of Radiology, University of Pennsylvania,
B6 Blockley Hall, 423 Guardian Drive, Philadelphia,
PA 19104-6069, USA
e-mail: intaelee@gmail.com

K. Shogen
Alfacell Corporation,
Somerset, NJ 08873, USA

Introduction

Ledoux first observed the anti-tumor effect of RNases A on Ehrlich carcinoma (ascites tumors) and spontaneous mammary carcinoma (solid tumors) in vivo [10, 11]. He found that homologs of ribonucleases isolated from amphibian eggs and embryos had greater cytotoxic activity than RNase itself. As an RNA targeting agent, ranpirnase (ONCONASE®: ONC) is the smallest member of the RNase A superfamily, with 104 residues as compared to the 124 in the primary structure of RNase A and molecular mass of 11.8 kDa [1]. ONC is also a basic single chain and stable protein. ONC has been successfully moved into translational research with clinical testing in the United States and Europe [3, 17]. The anti-cancer mechanisms of ONC are not yet fully understood. ONC first interacts with the plasma membrane surface. Then, ONC is internalized by endocytosis. Although the mechanism of bilayer transverse is not known, ONC is released into the cytosol of the tumor cells, where it selectively degrades t-RNA beyond repair [5, 21]. It was also reported that 24–48 h after

incubation is needed to enhance the cytotoxicity and inhibit protein synthesis by ONC [4, 20].

Using A549 non-small cell lung carcinoma (NSCLC) xenografts, we recently reported that a single administration of ONC showed significant tumor growth retardation in the presence and absence of cisplatin, one of most commonly used chemotherapeutic agents in the clinic [15]. We also performed animal toxicology studies with ONC, $LD_{10(30)} = \sim 12.5$ mg/kg and $LD_{50(30)} = \sim 15$–17.5 mg/kg. The maximum tolerated dosage for a single injection of ONC was ~ 10 mg/kg. For expanding to the clinic, we studied the toxicology of multiple administrations of ONC. We found that small dosages with repeated i.v. administrations of ONC (i.e., twice a week), the $LD_{50(30)}$ value was significantly elevated. ONC at 15 mg/kg (2.5 mg/kg, twice per week for 3 weeks) did not show the typical negative symptoms (no weight loss). Thus, we were encouraged to study the tumoricidal efficacy of small multiple dosages of ONC in A549 NSCLC xenografts.

ONC increased growth delay in Du145 tumor in vivo, due to ONC-induced increases in delivery and penetration into tumor regions resulting from ONC-induced reduction in tumor hypertension and increased tumor blood flow [13, 16]. Kim et al. [7] reported that a single administration of ONC enhanced the radiation response of A549 human NSCLC, likely due to reduced O_2 consumption (QO_2) and increased apoptosis, in addition to the mechanisms observed by various investigators [19, 20]. In this work, we studied whether ONC induced apoptosis in vivo in the gefitinib-induced apoptosis-resistant A549 human NSCLC cell lines. Whether the mono-therapy with ONC via multiple small-dosage administrations could inhibit tumor growth in A549 tumors in vivo was studied. We also preformed histological studies for hematoxylin and eosin (H & E) staining, apoptosis studies with TUNEL labeling, and caspase-3-antibody labeling after ONC treatments.

Dynamic contrast-enhanced magnetic resonance imaging (DCE-MRI) has shown promise as a method for evaluating of tumor vasculature and monitoring the efficacy of anti-vascular and anti-angiogenic therapies [9]. This particular DCE-MRI method was utilized to non-invasively monitor the action of the therapeutics in early-stage clinical trials [9]. K^{trans} reflected contrast delivery [perfusion and transport across the vascular endothelium (permeability)], with the dominant factor depending on whether delivery was flow or permeability limited. Using a DCE-MRI method, we studied whether the therapeutic outcome of ONC could be predicted on our tumor model. Our hypothesis was that the increases in K^{trans} would be an indicator of response to ONC. The parameter, K^{trans}, as dynamic T_1-weighted spin echo pulse sequence was chosen and recorded for DCE-MRI perfusion [25].

Materials and methods

Cell lines

Frozen A549 human NSCLC and HLF-1 human lung fibroblast cell lines were purchased from the American Type Culture Collection (Rockville, MD, USA), thawed, cultured, and grown in vitro. Both A549 and HLF-1 cells were maintained at 37°C for the duration of the experiments. The cells grew in RPMI-1640 medium supplemented with 15% fetal bovine serum (FBS), 10–25 mM HEPES buffer, 5 mM L-glutamine, and antibiotics (15% FBS-RPMI-1640).

Preparation of ONC

ONC (trademark: Onconase® and generic name: ranpirnase) was supplied by the Alfacell Corporation (Bloomfield, NJ, USA). Original stock solutions of ONC at 5 mg/ml were made in sterile distilled water and frozen at −20°C until needed. Prior to experiments, ONC was thawed and diluted to the appropriate concentrations in medium for in vitro studies and saline for in vivo.

Clonogenic survival and proliferation assay for in vitro response to ONC

For the proliferation studies, the appropriate cell number (2.5×10^4) of A549 tumor or HLF-1 human lung fibroblast cells was plated into six-well plates. The next day, ONC at 0–10 μg/ml was added into the wells. The status of proliferation was observed and photographed on a daily basis. For the clonogenic survival studies, the appropriate cell number (from 100 to 1×10^4) of A549 tumor cells were then incubated at 37°C for 5 h to allow for cell attachment and then incubated for various time exposures with 0–10 μg/ml ONC. The six-well plates were rinsed twice with RPMI-1640 medium to remove the ONC from the medium. After exposure to ONC, clonogenic assays were performed as described elsewhere [13], 7 ml of 15% FBS-RPMI-1640 was then added to six-well plates and cells were allowed to grow for 8–9 days. Cultures were fixed with 99.5% isopropyl alcohol, stained with 1% crystal violet and counted. Colonies with more than 50 cells were scored as positive.

Animals bearing tumors

Animal care was in compliance with all rules as set by the University of Pennsylvania for the care and use of laboratory animals, with standards equivalent to the UKCCCR

guidelines for the welfare of animals in experimental neoplasia. Eight- to 10-week-old female athymic NCR-nu/nu nude mice (purchased from the NCI, Bethesda, MD, USA) bearing human tumor xenografts of A549 human NSCLC cells were utilized. Tumors were induced by injecting viable cells (2×10^6) suspended in 50 µl of RPMI-1640 medium subcutaneously into the right thighs of mice.

Histological study procedures

For histological preparation of A549 tumors, animals with established tumors of 8–9 mm diameter were i.v. injected with ONC at 2.5 mg/kg, twice a week (on Monday and Thursday) for 2 weeks. At day 3 after the last injection of ONC or saline, the animals were sacrificed by injection of a mixture of ketamine/xylazine (90/9 mg/kg i.p.), followed by cervical dislocation. The tumor and kidney were excised from animals, then tumor and kidney samples were placed in 10% neutral buffered formalin overnight for fixation, and then sent to the Pathology Core at the Children's Hospital of Philadelphia (Abramson Research Center & CHOP, Philadelphia, PA, USA) for the histological studies. Once the tissues had been fixed, they were processed into paraffin blocks and made into thin microscopic sections using a microtome, then placed on slides. Routine H & E staining was performed on formalin fixed paraffin embedded tissues. Histological and morphological changes induced by ONC on tumor tissues and kidney were compared to the saline treated controls. Separately, slides were prepared and processed for caspase-3 antibody labeling, and TUNEL staining. These slides were evaluated by microscopy for determining the status of apoptosis. At least 200 cells were counted from each of three independent experiments, and the data are reported as the percentage of apoptotic cells.

Animal preparation and data acquisition by MRI

All MR images were acquired with a 4.7-T $^{\text{UNITY}}$INOVA spectrometer (Varian Medical Systems, Palo Alto, CA, USA). For in vivo studies, mice were placed inside a ^{1}H linear polarized birdcage RF coil with an inner diameter of 5 cm. The tumor volume was ~300–400 mm^3. Prior to the MR imaging protocol, a catheter was inserted into the tail vein of the mouse for injection of the contrast agent (Gd-DPTA). The second catheter was i.p. inserted for injection of ONC. The animal was sedated with isoflurane through a nose cone. Its core temperature was monitored by a rectal thermistor and maintained at 37°C by a flow of warm air. The electrocardiogram (ECG) was also monitored by attaching a pair of subdermal needle electrodes. The protocol for the T_1 mapping included a multi-slice various flip angle gradient echo pulse sequence with echo time (TE)/repetition time (TR) of 2.1/200 ms, flip angles of 0 ~ 180°, a matrix size of 128 × 64 (frequency direction × phase direction), field of view (FOV) of 4 cm × 2 cm (frequency direction × phase direction), a slice thickness of 2 mm, and total acquisition time of 6 min 37 s. Dynamic T_1-weighted spin echo pulse sequence was recorded for dynamic contrast-enhanced MRI perfusion with the following parameter settings: TE/TR 8.5/200 m, matrix size 128 × 64, FOV 4 × 2 cm, slice thickness 2 mm, total slice number 12 (kidney slice five, tumor slice seven), pixel size 0.3125 × 0.3125 × 2 mm, time resolution 12.8 s, total number of dynamic images 300 per slice, total imaging time 64 min, single acquisition, same field of view as the T_1 map protocol, and same matrix as the T_1 map protocol. A bolus injection of Gd-DTPA was followed by ten pre-acquisitions.

Contrast agent, Gd-DTPA, concentrations in plasma and tissue

Gd-DTPA(Omniscan$^{\text{TM}}$, Amersham Health) was diluted to 50 mM, then infused as a bolus injection at 0.5 mmol/kg on a secured connection with a catheter into the tail vein.

The bolus injection of Gd-DPTA was done over ~12 s to maintain the heart rate of each animal. Plasma concentration for Gd-DPTA was calculated by comparing changes in signals of the ROI of vena cava from the MRI slices of the kidney. We calculated plasma concentration for each animal by calculating signal changes using Eq. 1.

$$\frac{S_t}{S_o} = e^{-TE \cdot R_2 \cdot (1-h) \cdot C_p} \frac{1 - e^{-TR\left(\frac{1}{T_{10}} + R_1(1-h)C_p\right)}}{1 - e^{-TR/T_{10}}} \quad (1)$$

S_0 is the signal in the absence of Gd-DPTA ($C_t = 0$), and S_t is the signal after an injection of Gd-DPTA. C_p is plasma concentration, h is hematocrit ($h = 0.45$, no unit), TE/TR is echo time/repetition time, R_1/R_2 is the longitudinal relaxivity/the transverse relaxivity, T_{10} is the value of T_1 prior to an injection of Gd-DPTA.

The calculated C_p curve was fitted using a clearance model as shown in Eq. 2.

$$C_p = D \cdot [a_1 \cdot \exp(-m_1 t) + a_2 \cdot \exp(-m_2 t)] \quad (2)$$

D is the Gd-DPTA dose (mmole per kilogram body weight of the experimental animal), and the clearance is described by m_1, m_2 which are their rate constants corresponding to the distribution and clearance phases, respectively (min^{-1}). a_1, a_2 are the amplitudes of the components (kg l^{-1}) [24, 25].

The calculated C_t curve was fitted using a clearance model as shown in Eq. 3. C_t is Gd-DPTA concentration in tissue, concentration of blood plasma with respect to

hematocrit level. Tissue concentration curve was obtained by utilizing an optimal Müller's algorithm to get the root.

$$\frac{S_t}{S_o} = e^{-TE\cdot R_2\cdot C_t}\frac{1-e^{-TR\left(\frac{1}{T_{10}}+R_1\cdot C_t\right)}}{1-e^{-TR/T_{10}}} \quad (3)$$

Kinetic model

Image analysis of the dynamic contrast-enhanced (DCE) data was based on the generalized kinetic model developed by Tofts [24, 25]. This model predicts the changes in concentration of the contrast agent in the tissue due to its transfer from the plasma into the interstitial space and back.

$$C_t = D\cdot K^{\text{trans}}\sum_{i=1,2} a_i\frac{\exp(-K^{\text{trans}}t/V_e)-\exp(-m_i t)}{m_i - K^{\text{trans}}/V_e} \quad (4)$$

K^{trans} is the volume transfer constant between blood plasma and extravascular extracellular space (EES unit is min^{-1}), V_e is the EES fractional volume (the volume of EES per unit volume of tissue).

The time course of signal enhancement during 60 min after the bolus injection was analyzed at pixel resolution using a nonlinear Levenberg–Marquardt least-square fitting algorithm.

Retardation in tumor growth in vivo after treatment with multiple small-dosage administrations of ONC

Experiments were carried out (~4 weeks after tumor implantation) when the tumor volume was between 200 and 400 mm^3. Tumors were measured with a caliper 2–3 times a week for up to 60 days after treatments. Tumor volumes were calculated using the formula $V = 0.4 \times AB^2$, with A and B as the longer and shorter diameters of the tumor, respectively [13]. For the in vivo ONC treatment, ONC was dissolved in sterile 0.9% NaCl solution before injections. The mice were repeatedly given an intravenous (i.v.) injection of ONC at 2.5 mg/kg per administration (twice a week for 1–3 weeks) at a volume of 0.1 ml/20 g of body weight.

Measurement of interstitial fluid pressure from tumor and normal tissue (skeletal muscles and kidney)

Interstitial fluid pressure (IFP) was measured with the Win technique using 23-gauge needles with a side-hole 2 mm from the tip. Measurements were made by introducing WIN needles into the central regions of the tumors (located in the right hind-limb) and skeletal muscles (located in the left hind-limb) or left kidney during 2 h of observation after the ONC treatment. All IFPs were measured for 2 h after an i.v. injection of ONC at 5 mg/kg using two or three WIN needles (two for tumor and skeletal muscles, one for the left kidney in a separate animal). The signal was amplified and connected to a MacLab/4e analog digital system (ADInstrument, Milford, MA, USA) [12, 13].

Statistical evaluation

All measured values were presented as the mean ± SE of each group. Significant differences within a group before and after ONC treatment were evaluated using a paired t test. Differences between treatment groups were evaluated with an unpaired t test. For statistical evaluation of K^{trans} values before and after the ONC treatment, K^{trans} values were obtained from seven slices per tumor using an MRI method. The median of K^{trans} values was calculated for each tumor. The mean of all median K^{trans} values was used for the statistical analysis, and the groups were compared using a t test. Significance was set at 95% ($P = 0.05$) for all analyses.

Results

The cellular proliferation rate of A549 tumor cells was significantly inhibited by ONC at 10 μg/ml (for 3 days exposure) compared to the untreated control (first row-control vs. second row-ONC in Fig. 1a, b vs. e, f). We were able to observe membrane blebbing at high magnifications (×200). In contrast, there was no difference in cellular proliferation between the untreated control and ONC-treated groups in HLF-1 human lung fibroblast (Fig. 1c, d vs. g, h). In order to determine the cytotoxic effect of ONC on A549 tumor cell lines (Fig. 1i), a clonogenic assay was performed after incubation with ONC. $SF_{0.5}$ (surviving fraction at 50%) after 24 h was ~5 μg/ml and that after 72 h was ~2 μg/ml. $SF_{0.1}$ (surviving fraction at 10%) after 72 h was ~5 μg/ml, so the survival fraction was dramatically decreased by ONC.

Tumor growth delay is defined as the time for a treatment group minus the controls to reach a fourfold volume increase. Saline-treated control tumors took 10.2 ± 0.8 days for a fourfold volume increase, which established the baseline measurement (Fig. 2). Three case studies were made to observe the influence of ONC and single and multiple dosages. We first i.v. injected the animals with ONC at 2.5 mg/kg; a fourfold increase in tumor volume took 12.9 ± 1.4 days, resulting in a growth delay of 2.7 days (vs. control, $P = 0.18$), where an i.v. injection of ONC at 2.5 mg/kg alone did not effectively retard the tumor growth

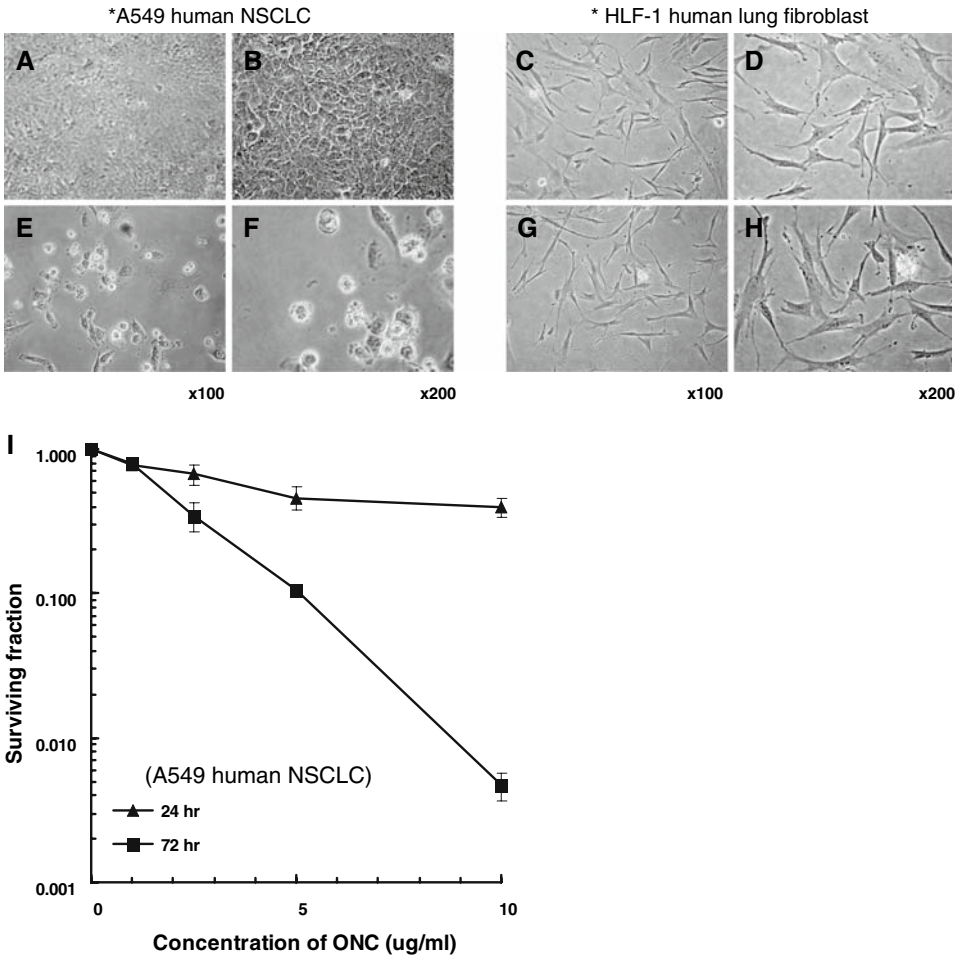

Fig. 1 ONC significantly inhibited the proliferation on A549 human NSCLC cells (**a**, **b**, **e**, **f**), but not on HLF-1 human lung fibroblast (**c**, **d**, **g**, **h**). The treatment procedure was followed, as described in Materials and methods. The photographs were taken at day 3 after the ONC treatment, ONC at 0 μg/ml in the first row (**a**, **b**, **c**, **d**) and ONC at 10 μg/ml in the second row (**e**, **f**, **g**, **h**). **i** The survival curve for the cytotoxic effect of ONC on A549 human NSCLC cell lines. The clonogenic assay was performed after different incubation durations (24 or 72 h) with ONC

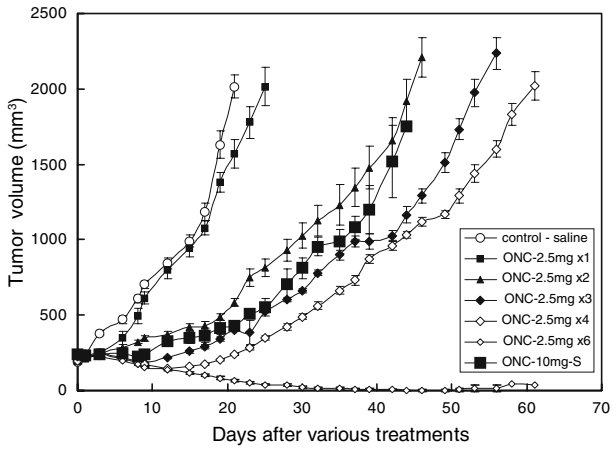

Fig. 2 Significant retardation in tumor growth was observed by multiple small dosages of ONC (mean volume of five tumors, bars, ±SE). The volume of A549 tumors in the right hind legs of athymic nude mice are shown as a function of days after dosage of ONC at 0 mg/kg (control *open circles*), 2.5 mg/kg (*closed squares*), 2.5 mg/kg × 2 (*closed triangles*), 2.5 mg/kg × 3 (*closed diamonds*), 2.5 mg/kg × 4 (*open diamonds*), 2.5 mg/kg × 6 (*small-open diamonds*) and 2.5 mg/kg × 4 (*big-closed squares*)

of A549 tumors. Then, when the animals were i.v. injected with ONC at 2.5 mg/kg, twice per week for a week (labeled as 2.5 mg/kg × 2), the tumor volume increased four times in 25.8 ± 2.0 days, giving us a growth delay of 15.6 days (vs. control, $P < 0.05$). We i.v. injected the animals with ONC at 2.5 mg/kg, twice per week for 2 weeks (labeled as 2.5 mg/kg × 4), the tumor volume increased four times in 38.8 ± 0.7 days, giving us a growth delay of 28.6 days. Lastly we i.v. injected the animals with ONC at 2.5 mg/kg, twice per week for 3 weeks (labeled as 2.5 mg/kg × 6). After the last injection of ONC, the tumor significantly regressed for 20–30 days, then some of the tumors slowly started to grow, but never reached a fourfold volume increase during the ∼60 days of the growth delay assay. Additionally, 40% of tumor xenografts were cured during ∼90 days observation. As a result, we could not perform the data analysis for the tumor growth delay for this treatment (labeled as 2.5 mg/kg × 6). We plan to perform tumor control studies using multiple small dosages of ONC, but it is beyond the scope of this paper. Thus, multiple i.v. administrations of ONC significantly inhibited the tumor growth of

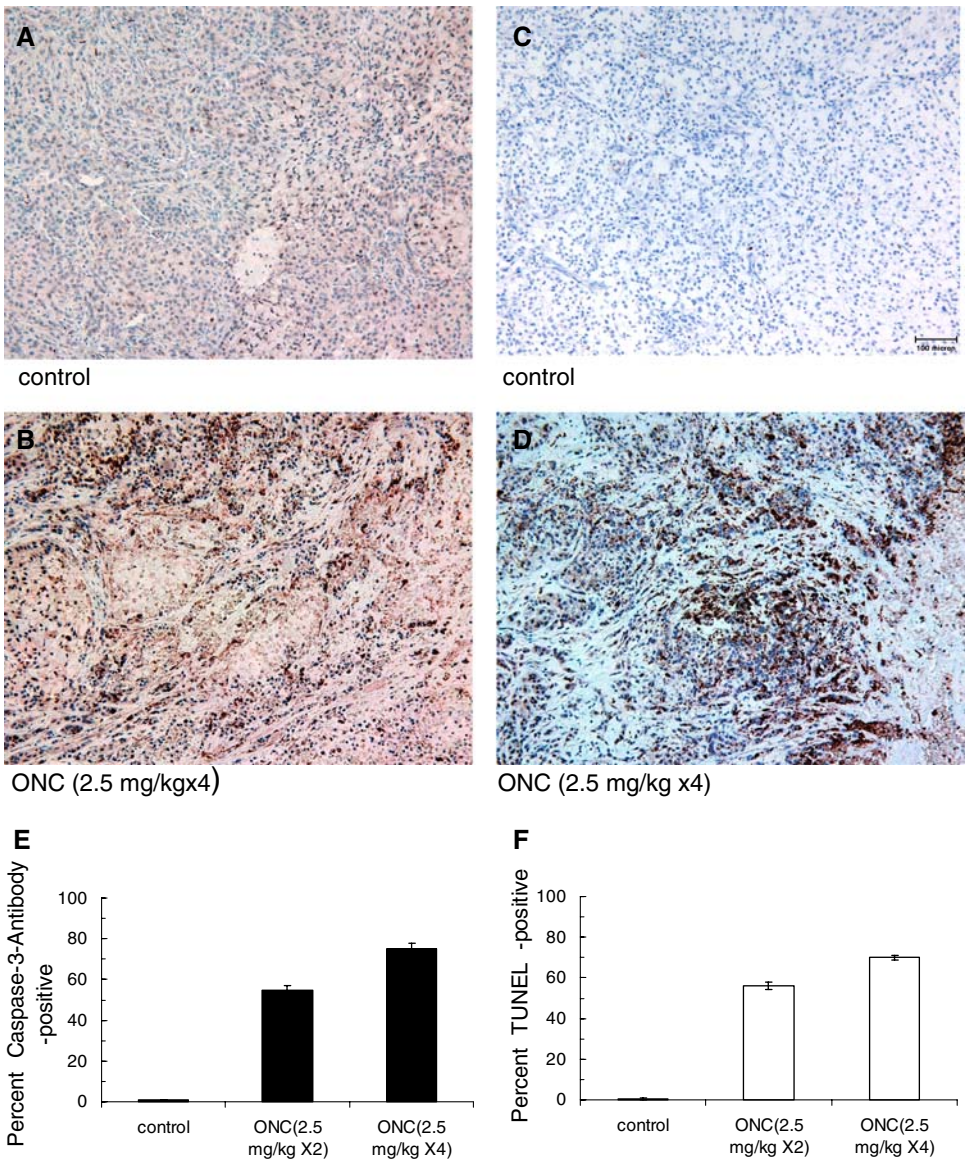

Fig. 3 ONC strongly induced apoptosis in A549 human NSCLC in vivo. Histologic evaluation of A549 tumors in animals treated by i.v. administrations of saline (**a**, **c**) or ONC at 2.5 mg/kg (**b**, **d**), twice per week for 2 weeks. Tumors were excised from the animals, 3 days after the last administration of saline or ONC, and fixed with 10% buffered formalin, as described in Materials and methods. The first column is for caspase-3 antibody labeling (some of apoptosis are shown as *dark-colored regions*), and the second column is for TUNEL staining (*darker regions* indicate greater levels of apoptosis). The first row represents 3 days after the last i.v. injection of saline and the second row shows 3 days after the last injection of ONC at 2.5 mg/kg (twice per week for 2 weeks; labeled as 2.5 mg/kg × 4). Positive-apoptotic cells were quantified. Significant increases in apoptosis by ONC (**e**, **f**)

A549 without any reduction of body weight compared to the saline-treated control group. In contrast, a single i.v. administration of ONC at 10 mg/kg was significantly and effectively tumoricidal in A549 tumors, reaching a growth delay of 22.6 days (the tumor volume increased four times in 32.8 ± 2.8 days; vs. control, $P < 0.05$), but with a ~15% reduction in body weight for 10–15 days before returning to the pre-treated values.

In this work, we verified whether ONC-induced apoptosis in vivo, as this may have been one of the mechanisms for reducing the tumor volume. The ONC-induced apoptosis was observed in A549 tumors in vivo using two immuno-histological methods of caspase-3 antibody labeling and TUNEL labeling (Fig. 3). We chose an apoptosis observation time at day 3 after saline (as a control) or ONC treatment, based on our previous observations that the occurrences of apoptosis became observable at day 3 after an i.v. administration of ONC [15]. We observed small occurrences of apoptosis in untreated A549 tumors in vivo (Fig. 3a, c). However, there was a significant increase in apoptosis by ONC (Fig. 3b, d). As shown in Fig. 3e, the percent caspase-3-antibody-positive cells were significantly increased from 1.0 ± 0.1 to 54.6 ± 2.3% ($N = 3$, $P < 0.05$; for ONC at 2.5 mg/kg × 2) and 74.8 ± 2.8% ($N = 3$, $P < 0.05$; for ONC at 2.5 mg/kg × 4). Also, the percent TUNEL-positive cells were significantly increased from 0.5 ± 0.3 to 55.9 ± 1.8% ($N = 3$, $P < 0.05$; for ONC at 2.5 mg/kg × 2) and 70.1 ± 1.1% ($N = 3$, $P < 0.05$; for ONC at 2.5 mg/kg × 4), respectively (Fig. 3f).

The measurements of the plasma and tissue concentration curve, K^{trans} and V_e map, and MRI data processing were done sequentially (Fig. 4a, b). The critical factor was

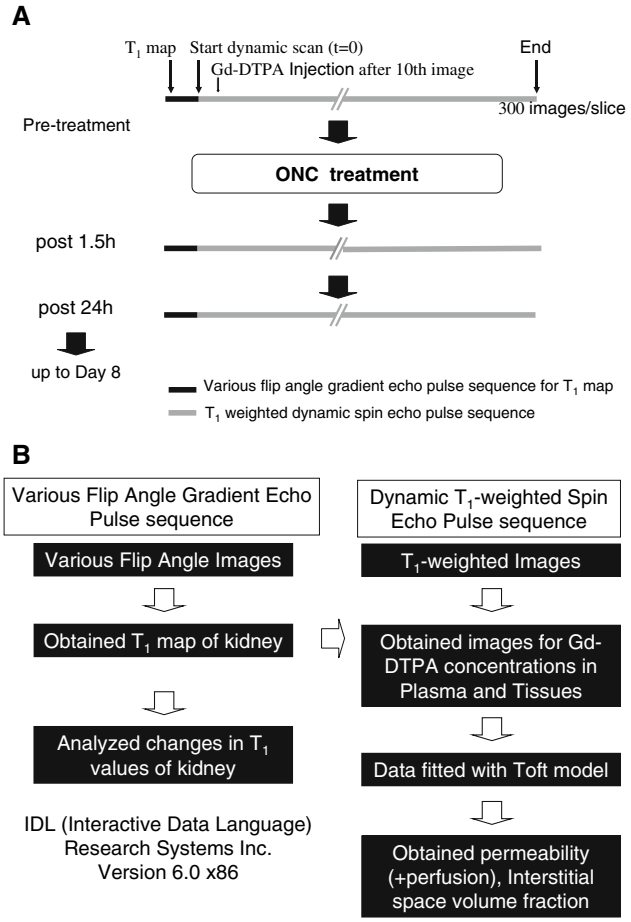

Fig. 4 **a** Scheme for the MRI images after treatment with ONC. Animals were prepared for two cannulations (an i.v. cannulation for MRI-contrast agent, Gd-DPTA, and an i.p. cannulation for ONC). Prior to treatment with ONC, T_1 maps of both tumor regions and kidney were constructed as a control. The dynamic scan (as $t = 0$ min) was started and Gd-DPTA was i.v. given after tenth image, then 300 images/slice were taken. At the several time points (1.5, 24 h, up to day 8) post-treatment with ONC via an i.p. route, the same imaging procedure was repeated to get T_1 maps of the tumor and kidney regions. **b** MRI data processing

to obtain the changes in the concentration of Gd-DPTA in the vena cava of the animal over the duration of the study of each animal. The plasma concentration curve from each dynamic scan was analyzed, which provided minimum error compared to the ideal plasma concentration curve. By DCE-MRI using a diffusible MRI contrast agent of Gd-DPTA, we monitored the effect of ONC on tumor perfusion. The follow-up MRI images at 1.5 h post-injection of ONC are shown in Fig. 5. The increases in the K^{trans} value of tumor regions are shown in red. In all four rows from A to D, red colored areas were accumulated at the rim of the tumor regions (2 mm in slice thickness; seven slices per tumor). The mean of the K^{trans} median values from four tumors was significantly altered by a 49.3 ± 7.5% increase ($N = 4$ mice, $P < 0.05$) from 0.0812 ± 0.014 (for the pre-ONC) to 0.1237 ± 0.0279 (for the post-ONC).

The imaging construction of the kidney was performed as shown in Fig. 6a, b, c. The kidney images were constructed non-invasively and repeatedly performed up to day 8. A subsequent T_1 map of the kidney (darker regions indicate less fluid) showed that T_1 values were decreased after treatment with ONC (Fig. 6d). This indicated that ONC caused temporary dehydration of the kidney, for up to 2 days post-treatment. It fully recovered around 4 days after ONC treatment. We could not find any difference in the structure of kidney by H & E staining method (Fig. 6e, f vs. g, h), indicating no long term side effects due to ONC.

As shown in Table 1, tumor interstitial fluid pressure (TIFP) of A549 tumors was 13.5 ± 0.8 mmHg for the untreated control animal. The IFP of the normal skeletal muscles (the counter part of tumor tissues) was −2.0 ± 0.8 mmHg. So, we observed that TIFP of the human xenografts in nude mice was significantly elevated compared to the normal skeletal muscles. This elevated TIFP was effectively reduced to 4.5 ± 0.8 mmHg by ONC during 2 h observation after an i.v. administration of ONC at 5 mg/kg. In contrast, the IFP values of skeletal muscles and kidney was not altered by ONC.

Discussion

The main limitation of anti-neoplastic chemotherapy is mainly due to the inability of cytotoxic agents to differentiate between normal and malignant cells [2, 8, 18]. To reduce the toxicity in clinical situations, most chemotherapeutic agents are distributed by multiple small dosages. Unfortunately, this also reduces anticancer efficacy. In this investigation, we studied what effects ONC had on normal and malignant cells (i.e., HLF-1 human lung fibroblast cells vs. A549 human NSCLC cells). In Fig. 1, there was differential effect of ONC between normal and malignant cells. It was also reported that A549 human NSCLC cell lines were the gefitinib-induced apoptosis-resistant [22, 23]. We also studied the tumoricidal effectiveness and the severity of side effects after the multiple small dosages of ONC.

Remarkable increases in apoptosis were observed after multiple small-dosage injections of ONC using caspase-3 antibody labeling and TUNEL labeling assay in vivo as shown in Fig. 3. The percentage of TUNEL-positive cells significantly increased from 0.5 ± 0.3 to 55.9 ± 1.8% (after 1 week of treatment) and to 70.1 ± 1.1% (after 2 weeks), respectively. It is probably a main reason for the effectiveness of multiple small-dosage injections of ONC for inhibition of tumor growth (Fig. 2). Additionally, multiple small-dosage injections did not cause a reduction

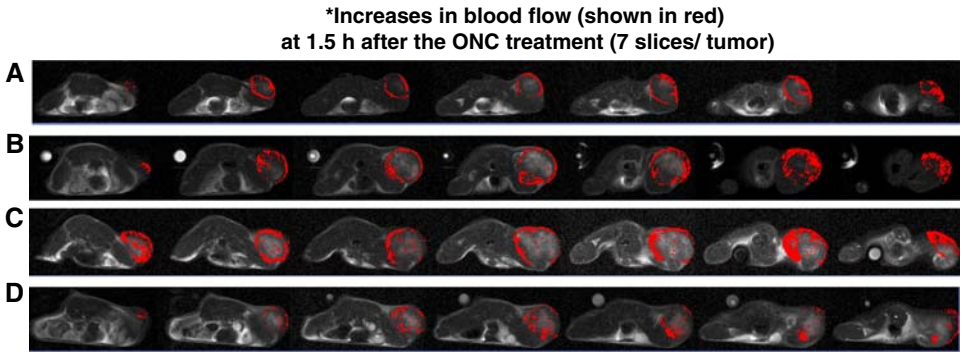

Fig. 5 K^{trans} map in A549 tumors after treatment with ONC. MRI images were taken by a 4.7T 50 cm horizontal bore spectrometer with 12.5 cm insert and 25 G/cm gradients. The dynamic scan (as $t = 0$ min) was started and Gd-DPTA was i.v. given after the tenth image, then 300 images/slice were taken. At 1.5 h post-treatment with ONC via an i.p. route, the same imaging procedure was repeated to obtain T_1 maps of the tumor and kidney regions. After the tenth image, Gd-DPTA was i.v. injected and 300 images/slice were constructed. Various flip angle gradient echo pulse sequence were used for T_1 measurement and a fast method for multi slice T_1 map. Gradient spoiler was used for eliminating transverse magnetization. Each tumor had seven slices (i.e., each thickness was 2 mm, and the total slice number for each tumor was 7). From the four tumors (**a**, **b**, **c**, **d**) significant increases in K^{trans} values were observed at the rim of the tumor regions at 1.5 h post-treatment with ONC (shown in *red*)

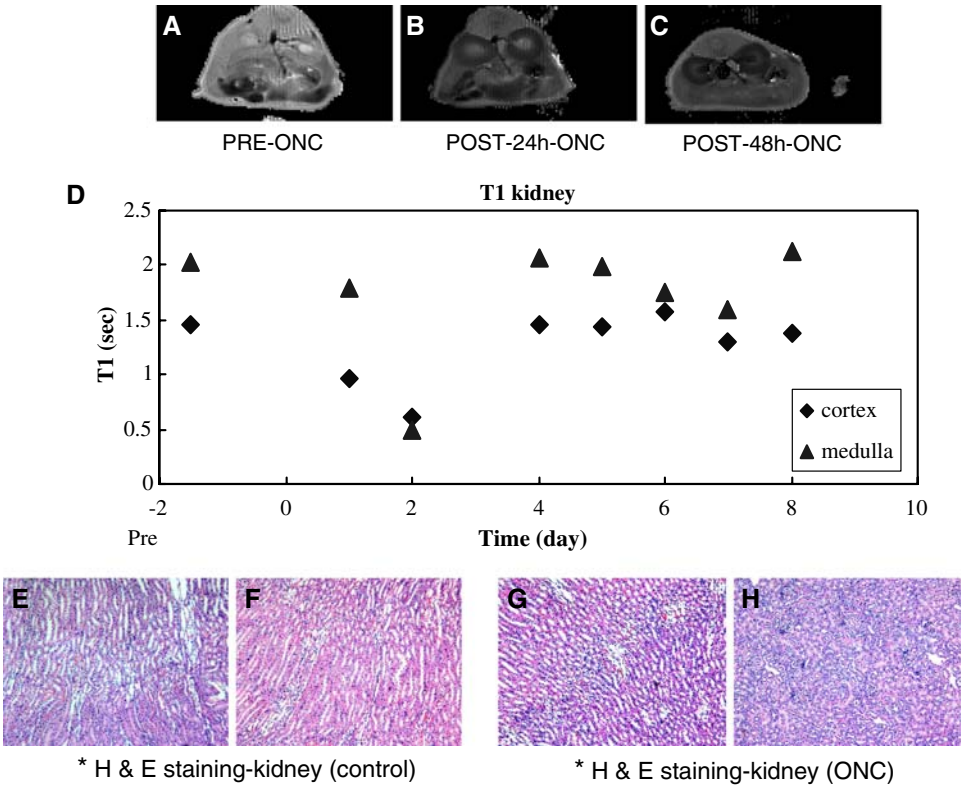

Fig. 6 ONC-induced reversible renal toxicity can be monitored non-invasively by MRI. The procedure for the MRI was performed, as described in Figs. 4 and 5. Prior to treatment with ONC, T_1 maps of the kidney (*darker regions* indicate less levels of fluid) were constructed as a control (**a**). The dynamic scan (at $t = 0$ min) was started and Gd-DPTA was i.v. given after the tenth image, then 300 images/slice were taken. Plot shows changes in T_1 values on the T_1 map of the kidney (**b**, **c**). Follow-up MRI images of the kidney were repeated 8 days after treatment with ONC (**d**; N = 2–5 mice per time point). We observed temporary dehydration in the kidney, but it fully recovered at ~4 days post-treatment of ONC. However, photographs of a kidney section taken from a mouse treated saline or ONC depict no pathological changes as measured by H & E staining (**e**, **f** vs. **g**, **f**)

in body weight (data not shown). Also, IFP was significantly reduced in A549 tumors (from 13.5 to 4.5 mmHg), but not in skeletal muscles and the kidney after a single i.v. administration of ONC (Table 1). The tumor interstitial fluid pressure (TIFP) values were ~1–2 mmHg after multiple small dosages of ONC at 2.5 mg/kg × 4 (data not

Table 1 Interstitial fluid pressure (IFP) before and after treatment with ONC in nude mice bearing human tumor xenografts ($N = 7$ mice)

Normal organs	IFP (mmHg)	2 h post-ONC
Skeletal muscle	−2.0 ± 0.5	−2.2 ± 0.7
Kidney (left)	2.1 ± 0.4	2.3 ± 0.5
Human tumor xenografts	TIFP ((mmHg))	2 h post-ONC
Du145, prostate	11.5 ± 0.6	5.0 ± 0.5
AsPC-1, pancreas	22.5 ± 0.9	5.2 ± 0.3
A549, lung	13.5 ± 0.8	4.5 ± 0.7

shown). We hypothesized that tumor vasculature could be normalized in this ONC treatment protocol, because apoptosis was induced by multiple small-dosages of ONC in tumor regions. The ONC-induced apoptosis reduced the TIFP and thus the tumor microcirculatory networks became normalized. This led to enhanced tumor oxygenation. This ONC-induced increase in tumor oxygen tension was previously reported [13, 16].

It is well documented that increases in viscous and geometric resistance to blood flow leads to elevated TIFP in solid tumors [6, 12]. The acute effect of ONC may be due to an ONC-induced reduction in viscous resistance (lowering of TIFP) in A549 tumors. In addition, due to inhibition of the cell proliferation and clonogenic cell survival of endothelial cells by ONC, the QO_2 was significantly reduced, making O_2 more available to the peripheral tissues. Previous studies confirm that ONC significantly reduced QO_2 [7, 14]. Moreover, in this investigation temporary increase in tumor blood flow was observed after treatment with ONC, particularly in the tumor periphery regions (Fig. 5).

ONC induced reversible renal toxicity that was monitored non-invasively by MRI. Changes in T_1 values on the T_1 map of the kidney were shown as temporary dehydration of the kidney (Fig. 6b, c). It was surprising to find that T_1 values on the T_1 map of the kidney of MRI was sensitive to the functional and transitional changes caused by a single injection of ONC at 5 mg/kg. The kidney fully recovered at ~4 days post-treatment of ONC (Fig. 6d). The reversible renal toxicity seems to be caused by the unusual stability of ONC [26]. However, histology photographs of a kidney section taken from a mouse treated with saline or ONC depicted no pathological changes measured by H & E staining (Fig. 6e, f vs. g, i). There are two possible types of changes in the kidney after ONC treatment; one is functional change and the other is structural change. Vasandani's studies showed that the nephrotoxicity was limited to the proximal tubules after daily i.p. injection of ONC at 0.44 mg/kg per day for five consecutive days in a week and treated for 3 weeks (total dosage of ONC was 6.6 mg/kg). However, the kidney completely recovered its structural damage 2 weeks after the conclusion of the 3-week ONC therapy.

In conclusion, ONC significantly inhibited tumor growth of A549 human NSCLC cells without damaging non-cancerous cells (HLF-1 human lung fibroblast). This is a new and attractive cancer treatment modality, since a functional p53 is not affected by RNA damage [20, 21]. Multiple small-dosages of ONC significantly inhibited tumor growth of A549 NSCLC xenografts with manageable toxicity, due to remarkably increased apoptosis during the ONC therapy. This investigation suggests important potential clinical uses of ONC for the treatment of NSCLC patients.

Acknowledgments This research was supported by Alfacell Corporation through their sponsorship research agreement with the University of Pennsylvania. The authors would like to express their thanks to Dr. Dae H. Kim's assistance on the MRI studies. The authors also appreciate Daniel Martinez at the Pathology Core, Children's Hospital of Philadelphia (CHOP), for his histological services for processing paraffin blocks and slides for the H & E staining, caspase-3 antibody labeling, and TUNEL staining studies.

References

1. Ardelt W, Mikulski SM, Shogen K (1991) Amino acid sequence of an anti-tumor protein from *Rana pipiens* oocytes and early embryos: homology to pancreatic ribonucleases. J Biol Chem 266:245–251
2. Beani CP (2000) Combined modality therapy for unresectable stage III non-small cell lung cancer: new chemotherapy combinations. Chest 117:127s–132s
3. Costanzi J, Sidransky D, Navon A, Goldsweig H (2005) Ribonucleases as a novel pro-apoptonic anticancer strategy: review of the preclinical and clinical data for ranpirnase. Cancer Invest 3:643–650
4. Grabarek J, Ardelt B, Du L, Darzynkiewicz Z (2002) Activation of caspases and serine proteases during apoptosis induced by onconase (ranpirnase). Exp Cell 278:61–71
5. Iordanov MS, Ryabinina OP, Wong J, Dinh TH, Newton DL, Rybak SM, Magun BE (2000) Molecular determinants of apoptosis induced by the cytotoxic ribonuclease onconase: evidence for cytotoxic mechanisms different from inhibition of protein synthesis. Cancer Res 60:1983–1994
6. Jain RK (2005) Normalization of tumor vasculature: an emerging concept in antiangiogenic therapy. Science 307:58–62
7. Kim DH, Kim EJ, Kalota A, Gewirtz AM, Glickson J, Shogen K, Lee I (2007) Possible mechanisms of improved radiation response by cytotoxic RNase, ONCONASE®, on A549 human lung cancer xenografts of nude mice. Adv Exp Med Biol 599:53–59
8. Kong FM, Zhao L, Hayman JA (2006) The role of radiation therapy in thoracic tumors. Hematol Oncol Clin North Am 20:363–400
9. Leach MO, Brindle KM, Evelhoch JL, Griffths JR, Horsman MR, Jackson A, Jayson GC, Judson IR, Knopp MV, Maxwell RJ, McIntyre D, Proce P, Rathbone R, Rutin GJ, Tofts PS, Tozer GM, Vennart W, Waterson JC, Williams SR, Workman P (2005) The assessment of antiangiogenic and antivascular therapies in early-stage clinical trials using magnetic resonance imaging: issues and recommendations. Br J Cancer 92:1599–1610

10. Ledoux L (1955) Action of ribonuclease on certain ascites tumours. Nature 175:258–259
11. Ledoux L (1955) Action of ribonuclease on two solid tumours in vivo. Nature 176:35–37
12. Lee I, Boucher Y, Jain RK (1992) Nicotinamide can lower tumor interstitial fluid pressure: mechanistic and therapeutic implications. Cancer Res 52:3237–3240
13. Lee I, Lee YH, Mikulski SM, Lee J, Covone K, Shogen K (2000) Tumoricidal effects of onconase on various tumors. J Sur Oncol 73:164–171
14. Lee I, Lee YH, Mikulski SM, Lee J, Shogen K (2000) Enhanced cellular radiation sensitivity of androgen-independent human prostate tumor cells by onconase. Anticancer Res 20:1037–1040
15. Lee I, Kalota A, Gerwirtz AM, Shogen K (2007) Antitumor efficacy of the cytotoxic RNase, ranpirnase, on A549 human lung cancer xenografts of nude mice. Anticancer Res 27:299–308
16. Lee I, Kim DH, Sunar U, Magnitsky S, Yodh AG, Shogen K (2006) The physiological mechanisms of ranpirnase-induced enhancement in radiation response on A549 human lung carcinoma xenografts in nude mice. Int J Radiat Oncol Biol Phys 66:s580–s581
17. Mikulski SM, Costanzi JJ, Vogelzang NJ, McCachren S, Taub RN, Chun H, Mittelman A, Panella T, Puccio C, Fine R, Shogen K (2001) Phase II trial of a single weekly intravenous dose of ranpirnase in patients with unresectable malignant mesothelioma. J Clin Oncol 20:274–281
18. Penketh PG, Shyam K, Sartorelli AC (1996) Mechanisms of resistance to alkylating agents in drug resistance. In: Hait WN (ed) Drug resistance, Kluwer, Boston, pp 65–81
19. Rutkoski TJ, Kurten EL, Mitchell JC, Raines RT (2005) Disruption of shape-complementary markers to create cytotoxic variants of ribonuclease A. J Mol Biol 354:41–54
20. Rybak SM, Newton DL (1999) Natural and engineered cytotoxic ribonucleases: therapeutic potential. Exp Cell Res 253:325–335
21. Saxena SK, Sirdeshmukh R, Ardelts W, Mikulski SM, Shogen K, Youle RJ (2002) Entry into cells and selective degradation of tRNA by a cytotoxic member of the RNase A family. J Biol Chem 277:15142–15146
22. Sordella R, Bell DW, Harber DA, Settleman J (2004) Gefitinib-sensitizing EFGR mutations in lung cancer activate anti-apoptotic pathway. Science 305:1163–1167
23. Tracy S, Mukohara T, Hansen M, Meyerson M, Johnson BE, Jaenne PA (2004) Gefitinib induces apoptosis in $EFGR^{L858R}$ non-small-cell lung cancer line H3255. Cancer Res 64:7241–7244
24. Tofsts PS, Kermode AG (1991) Measurement of the blood–brain barrier permeability and leakage space using dynamic MR imaging. 1. Fundamental concepts. Magn Reson Med 17:357–367
25. Tofsts PS, Brix G, Buckley DL, Evelhoch JL, Henderson E, Knopp MV, Larsson HBW, Lee T, Mayr NA, Parker GJM, Port RE, Taylor J, Weisskoff RM (1999) Estimating kinetics parameters from dynamic contrast-enhanced T1-weighted MRI of a diffusible tracer: standardized quantities and symbols. J Magn Reson Imaging 10:223–232
26. Vasandani VM, Burris JA, Sung C (1999) Reversible nephrotoxicity of onconase and effect of lysine pH on renal onconase uptake. Cancer Chemother Pharmacol 44:164–169